



# Significant improvements in dielectric, impedance, multiferroic and magnetoelectric properties of $(1 - x)\text{Co}_{0.5}\text{Ni}_{0.5}\text{Fe}_2\text{O}_4 - x\text{BaTiO}_3$ bulk composites ( $x = 0, 0.10$ and $0.20$ )

S. Shankar<sup>1,2</sup> , O. P. Thakur<sup>3,\*</sup>, and M. Jayasimhadri<sup>2,\*</sup>

<sup>1</sup> Experimental Research Laboratory, Department of Physics, ARSD College, University of Delhi, Dhaula Kuan, New Delhi 110021, India

<sup>2</sup> Luminescent Materials Research Lab, Department of Applied Physics, Delhi Technological University, Bawana Road, Delhi 110042, India

<sup>3</sup> Materials Analysis and Research Laboratory, Department of Physics, NSUT, Dwarka, New Delhi 110078, India

Received: 7 January 2021

Accepted: 18 May 2021

Published online:  
2 June 2021

© The Author(s), under exclusive licence to Springer Science+Business Media, LLC, part of Springer Nature 2021

## ABSTRACT

Magnetoelectric bulk composites of  $\text{Co}_{0.5}\text{Ni}_{0.5}\text{Fe}_2\text{O}_4 - \text{BaTiO}_3$  (CNFO–BT) were synthesized employing solid-state reaction method. The structural properties of CNFO–BT composites as discussed by X-ray diffraction method confirm lattice distortion and enlarged strain owing to BT substitution in CNFO. The dielectric and impedance measurements exhibit conventional Maxwell–Wagner polarization and confirm the existence of grain dominated non-Debye relaxation phenomena in CNFO–BT composites. The magnetic hysteresis curves reveal strong ferromagnetic behavior in all composites. The maximum energy storage density and an efficiency achieved for 0.8CNFO–0.2BT composite are  $4.25 \text{ mJ/cm}^3$  and 31.6%, respectively. The variation of polarization with magnetic field confirmed the highest magnetoelectric coefficient of  $5 \text{ mV/cm/Oe}$  for 0.8CNFO–0.2BT composite. The variation of dielectric permittivity and ferroelectric polarization with magnetic field reveals lattice distortion, interfacial charge polarization and restricted ferromagnetic domain wall rotation arising from substitution of BT in CNFO. These structure-dependent results suggest potential application of CNFO–BT composites in magnetoelectric sensors and energy storage devices.

## 1 Introduction

Multiferroics are the materials possessing two or more ferroic orderings, viz. ferroelectric, ferroelastic, ferromagnetic or ferrotoroidic [1]. The

magnetoelectric effect in multiferroics materials is ascribed by the magnetic induction of electric polarization and vice versa [2, 3] which makes them suitable for versatile applications such as magnetic memory devices, energy storage and magnetoelectric

Address correspondence to E-mail: ophthakur@yahoo.com; jayaphysics@yahoo.com

resonator [1, 4]. The extent of this coupling is limited in single-phase materials due to disparate origins of ferroic orderings [5]. Alternatively, the multiferroic magnetolectric composites are engineered artificially by mixing separately ferroelectric and ferromagnetic phases for enhancing the magnetolectric coupling at room temperature [5, 6]. Furthermore, the extent of coupling can be maximized by involving piezoelectric and/or piezomagnetic materials which acquaint in achieving strain-mediated coupling and good connectivity at the electric and magnetic phase [5].

Piezomagnetic spinel cobalt ferrite  $\text{CoFe}_2\text{O}_4$  is widely studied material exhibiting strong physicochemical properties owing to its statistical cationic distribution at octahedral/tetrahedral sites and magnetostriction [4, 7]. The unit cell of  $\text{CoFe}_2\text{O}_4$  (CFO) consists of face-centered cubic structure where 8 out of 64 and 16 out of 32 tetrahedral sites and octahedral sites are occupied by cobalt and iron ion, respectively. Due to their high electrical resistance and chemical stability, they are impeccably useful in magnetic storage devices, high-frequency circuits, waveguides and gas sensors [8]. In order to examine the enhanced multiferroic magnetolectric coupling and to induce the electric nature inside the magnetic spinel ferrite CFO, there is a need of some modifications. Significant efforts for improving the properties of CFO have been focused on partially substituting the  $\text{Fe}^{3+}$  ions [9, 10], composites with ferroelectric/piezoelectric materials [11], nanoparticles [12] and core/shell structures [13]. Among existing multiferroic magnetolectric systems,  $\text{CoFe}_2\text{O}_4$ – $\text{BaTiO}_3$ /PbTiO<sub>3</sub> composite systems are extensively reconnoitered [2, 4, 6, 14]. The lead-based composites show enhanced electrical properties; however, it is eco-friendly to use lead-free  $\text{BaTiO}_3$ -based composites [15, 16].  $\text{BaTiO}_3$  (BT) is the most appropriate suitable substitute for  $\text{PbTiO}_3$  due to its versatile polymorphic structure and excellent electrical properties [17, 18].

The properties of CFO are, however, always preparation as well as grain size dependent. CFO is hard ferrite, whereas  $\text{NiFe}_2\text{O}_4$  is soft ferrite [19]. The substitution of  $\text{Ni}^{2+}$  in the cubic structure of CFO is exciting as it alters the electrical properties and magnetic properties due to its lowered magnetic moment in comparison with  $\text{Co}^{2+}$  [20, 21]. This substitution renders Ni-CFO useful for vast applications with improved magnetolectric properties [22].

Theoretically strong ME coupling can be achieved if magnetocrystalline anisotropy in CFO is lowered [23]. The recent studies on  $\text{Co}_{0.5}\text{Ni}_{0.5}\text{Fe}_2\text{O}_4$  (CNFO) have revealed that strong magnetostatic interactions arising from different magnetocrystalline anisotropy are countered by increased coercivity and decreased magnetic saturation [6, 24, 25]. In addition, there have been investigations on  $\text{Co}_{0.5}\text{Ni}_{0.5}\text{Fe}_2\text{O}_4$ -based composites for existence of magnetolectric properties [1, 4, 14, 26]. The system of CNFO–BT has shown some promising results in magnetic and magnetolectric properties [22, 27–30]. Nonetheless, the origin of magnetodielectric, impedance and ferroelectric properties in  $\text{Co}_{0.5}\text{Ni}_{0.5}\text{Fe}_2\text{O}_4$ – $\text{BaTiO}_3$  composites with  $\text{Co}_{0.5}\text{Ni}_{0.5}\text{Fe}_2\text{O}_4$  as host material is not explored thoroughly. These composites are expected to bring improvements in electrical and magnetolectric properties in CNFO.

In this manuscript, composites of ferromagnetic  $\text{Co}_{0.5}\text{Ni}_{0.5}\text{Fe}_2\text{O}_4$  and lead-free ferroelectric  $\text{BaTiO}_3$  are prepared via solid-state reaction method. The effect of  $\text{BaTiO}_3$  on dielectric, impedance, multiferroic and magnetolectric properties of  $(1-x)\text{Co}_{0.5}\text{Ni}_{0.5}\text{Fe}_2\text{O}_4$ – $x\text{BaTiO}_3$  bulk composites ( $x = 0, 0.10$  and  $0.20$ ) has been studied extensively. These results are beneficial for exploiting lead-free CNFO–BT composites for magnetolectric and energy storage applications.

## 2 Experimental

### 2.1 Synthesis of $\text{Co}_{0.5}\text{Ni}_{0.5}\text{Fe}_2\text{O}_4$ and $\text{Co}_{0.5}\text{Ni}_{0.5}\text{Fe}_2\text{O}_4$ – $\text{BaTiO}_3$ composites

Bulk  $\text{Co}_{0.5}\text{Ni}_{0.5}\text{Fe}_2\text{O}_4$  and  $(1-x)\text{Co}_{0.5}\text{Ni}_{0.5}\text{Fe}_2\text{O}_4$ – $x\text{BaTiO}_3$  composites were prepared using high purity powders of  $\text{Co}_3\text{O}_4$ ,  $\text{Fe}_2\text{O}_3$ ,  $\text{NiO}$ ,  $\text{BaCO}_3$  and  $\text{TiO}_2$  employing solid-state reaction method. Stoichiometric amounts of chemicals for  $\text{Co}_{0.5}\text{Ni}_{0.5}\text{Fe}_2\text{O}_4$  (CNFO) and  $\text{BaTiO}_3$  (BT) were weighed mixed and ground using agate pestle mortar for 6 h. The mixture was calcined at  $1000^\circ\text{C}$  for 12 h in air. The powders of  $\text{Co}_{0.5}\text{Ni}_{0.5}\text{Fe}_2\text{O}_4$  and  $\text{BaTiO}_3$  were stoichiometrically mixed for preparing compositions  $(1-x)\text{Co}_{0.5}\text{Ni}_{0.5}\text{Fe}_2\text{O}_4$ – $x\text{BaTiO}_3$  with ( $x = 0, 0.10, 0.20$ ) and named as CNFO ( $\text{Co}_{0.5}\text{Ni}_{0.5}\text{Fe}_2\text{O}_4$ ), CNFO–10BT ( $0.9\text{Co}_{0.5}\text{Ni}_{0.5}\text{Fe}_2\text{O}_4$ – $0.1\text{BaTiO}_3$ ) and CNFO–20BT ( $0.8\text{Co}_{0.5}\text{Ni}_{0.5}\text{Fe}_2\text{O}_4$ – $0.2\text{BaTiO}_3$ ). The resultant powders were pressed into 10-mm-diameter pellets using polyvinyl alcohol as binder and sintered at  $1200^\circ\text{C}$  for 8 h along with

calcined powder of respective sample to avoid oxygen loss in sintering process.

## 2.2 Characterization techniques

The structural analysis has been carried out using Rigaku X-ray diffractometer employing Cu-K $\alpha$  radiation with wavelength of 1.5418 Å. The XRD data have been recorded from the powder obtained by crushing the sintered pellets. The pellets of CNFO–BT composites were silver coated to improve electrical contact. Dielectric and impedance measurements of the coated composite pellets were made using Wayne Kerr 6500 P high-frequency LCR meter setup in the frequency and temperature range of 100–1 MHz and 100–400 °C, respectively. The ferroelectric *P*–*E* hysteresis loop for the coated pellets was studied using Marine India *P*–*E* loop tracer setup operating at 50 Hz with electric field up to 5 kV/cm and magnetic field up to 4000 Oersted.

## 3 Results and discussion

The X-ray diffraction patterns of CNFO and CNFO–BT composites are shown in Fig. 1. The XRD plot of CFO is referred from our earlier work [4]. The XRD pattern of CNFO is matched with JCPDS # 22-1086 and confirms the spinel cubic structure with space group (*Fd3m*). The splitting and broadening of peaks in XRD of CNFO in comparison with XRD peaks of CFO at  $2\theta \sim 30^\circ$  and  $62.5^\circ$  are matched with JCPDS # 10-0325 for NiFe $_2$ O $_4$  [31] and are marked by ‘\*’ symbol in Fig. 1. This occurrence of NiFe $_2$ O $_4$  peaks confirms the formation of CNFO. The impurities in XRD of CNFO between  $2\theta$  of  $50^\circ$  and  $60^\circ$  are due to presence of Fe $_2$ O $_3$  and are matched with JCPDS # 02-0919. The XRD patterns of CNFO–BT system are matched with JCPDS # 22-1086 for CNFO and JCPDS # 05-0626 for BaTiO $_3$  (BT) and confirm the formation of CNFO–BT composites. The ferroelectric BT phase in the composite at  $2\theta \sim 32^\circ$  and at other higher values is indicated by ‘#’ symbol in Fig. 1.

The effect of BT addition in CNFO is observed by studying the lattice parameter variation and lattice strain estimations. The variation of lattice parameter was obtained using Debye–Scherrer equation [32] and lattice strain was obtained from Williamson–Hall equation [33], and the subsequent results are plotted in Fig. 2. It can be observed that the lattice parameter

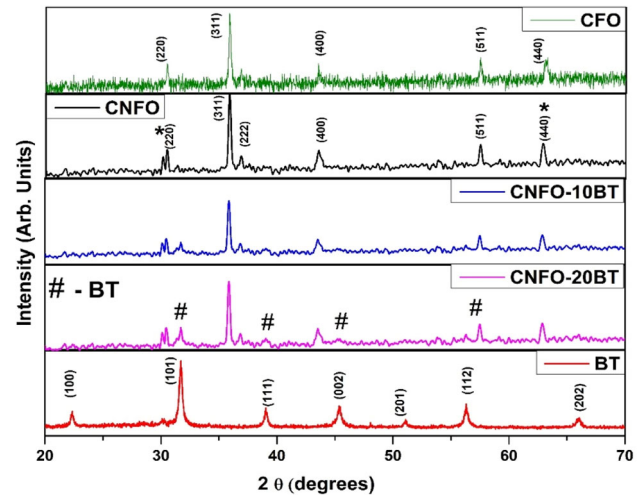


**Fig. 1** XRD patterns of CNFO and CNFO–BT composites

obtained for CNFO is 8.325 Å which is lower than that of CoFe $_2$ O $_4$  (10.7 Å) [4] as at both octahedral/tetrahedral sites, ionic radii of Ni $^{2+}$  (0.745/0.55 Å) are less than Co $^{2+}$  (0.69/0.58 Å) [34]. The lattice parameters in Fig. 2 decrease from 8.325 to 7.967 Å for CNFO to CNFO–BT composites due to lattice distortion arising on account of trapping centers formed by BT substitution. This lattice distortion is also accompanied by the increase in the lattice strain as shown in Fig. 2.

The dielectric analysis is an ideal technique for correlation of most of the properties of ferrites with preparation, composition and temperature. The frequency dependency of dielectric constant for CNFO and CNFO–BT composites is shown in Fig. 3a–c. The graphs show usual behavior of dielectric materials

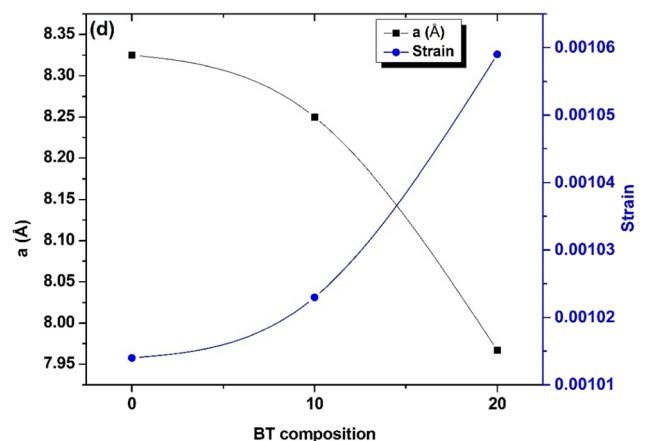


**Fig. 2** Variation of lattice parameter and strain in CNFO–BT composites with BT composition

with CNFO and CNFO–BT composites possessing large dielectric constant values [35] at low frequencies, and the dielectric constant decreases at higher frequencies.

The polarization mechanism of any dielectric material can be of the form of atomic, electronic, dipole and interface [36, 37]. The first two mechanisms, viz. electronic and atomic polarizations, usually have instantaneous effects and are observed at high frequencies only [36, 37]. The dipolar polarization in materials possessing polar groups is observed as step-like decrease in dielectric permittivity with frequency. The main reason to show such a decreasing trend is due to the presence of interfacial polarization as predicted by Maxwell–Wagner [38] and arises because of the charge accumulation on sample–

electrode interface as well as on the interface between the constituent phases [36, 37]. The exchange of electrons among multivalent  $Fe^{2+}/Fe^{3+}$  creates a spatial displacement of Fe ions along with electric field resulting in the polarization. The high value of dielectric permittivity at low frequencies is because of the presence of multivalent Fe ions, its related oxygen vacancies and defects. The decrement in the value of dielectric permittivity with frequency is because the dipoles cannot follow the electric field oscillations at higher fields. As per Koops theory, the contribution of dielectric constant at lower frequency originates from grain boundaries as they possess high impedance at grain boundary region [39]. The contribution to dielectric permittivity at high frequencies originates from low resistive grains. Thus, the presence of

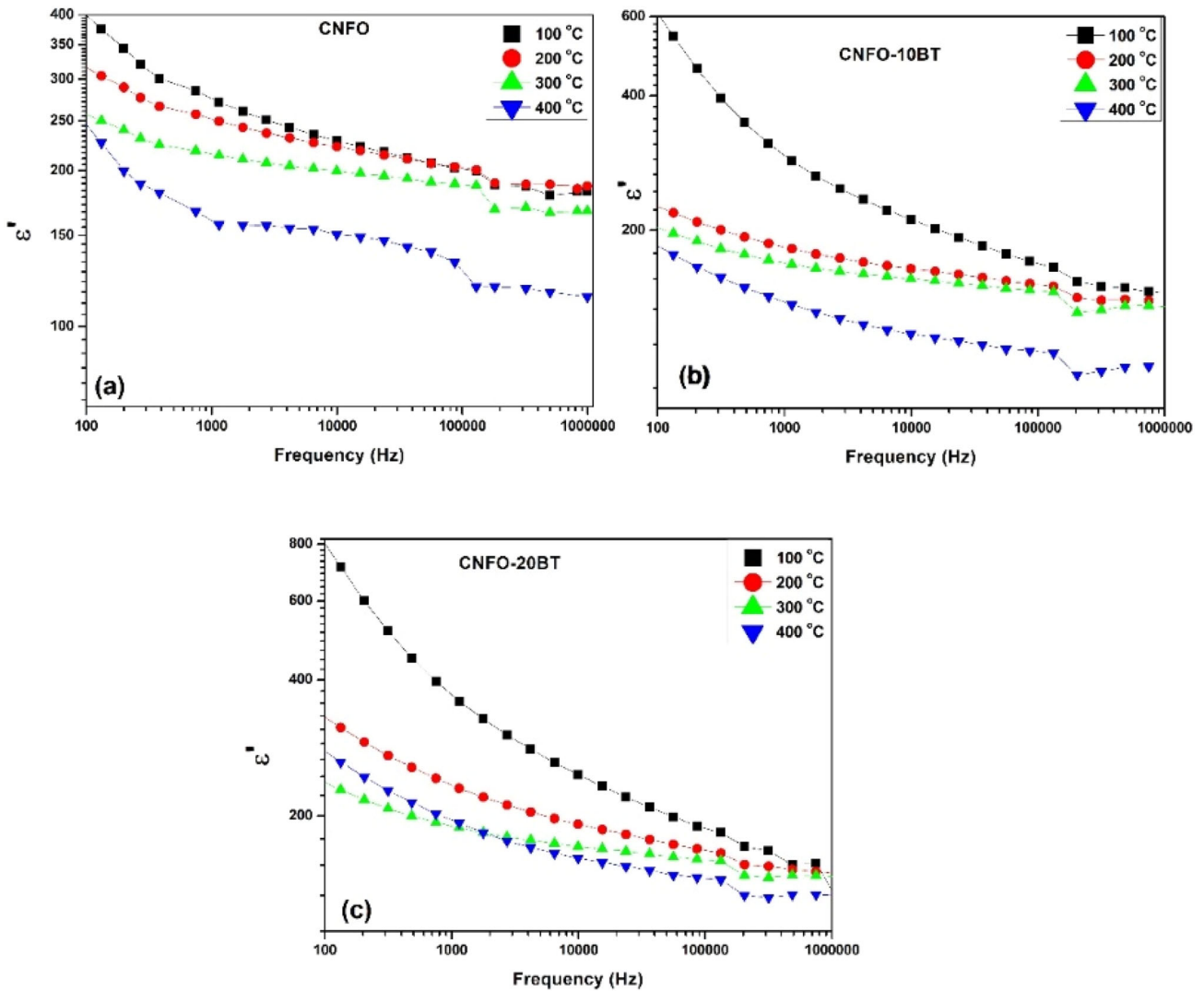


**Fig. 3** Frequency dependence of real part of dielectric constant ( $\epsilon'$ ) for CNFO and CNFO–BT composites at different temperatures

multivalent Fe ions is responsible for polarization in CNFO. The dielectric constant increases with BT content and suggests enhancement in electrical nature of CNFO–BT composites. For all composites, the increase in temperature from 100 to 400 °C onsets the space charge polarization linked to ionic defect movements and decreases the dielectric constant [40].

The magnetodielectric coupling constant (MD) is studied by measuring the dielectric properties at different magnetic fields and at a frequency of 10 kHz as shown in Fig. 4 and is quantified as

$$\text{MD} = \frac{\epsilon'(H) - \epsilon'(0)}{\epsilon'(0)} \times 100 \quad (1)$$

The composition of magnetic–ferroelectric phase is an important factor for deciding the magnetodielectric response. The variation in dielectric constant is less for CNFO and significantly increases with BT content. This enhancement could be possibly due to the modification of spatial charge distribution and restricted ferromagnetic domain wall rotation originating from BT substitution in CNFO. With increasing magnetic field, the change in dielectric constant drastically decreases due to alignment of domain walls in CNFO. Surprisingly, all CNFO–BT composites indicate stability in magnetodielectric coupling by displaying non-zero MD value at even higher fields. It is important to note that the magnetodielectric response in CNFO as well as CNFO–BT composites originates due to the contribution of magnetostriction of CNFO. This occurs due to the

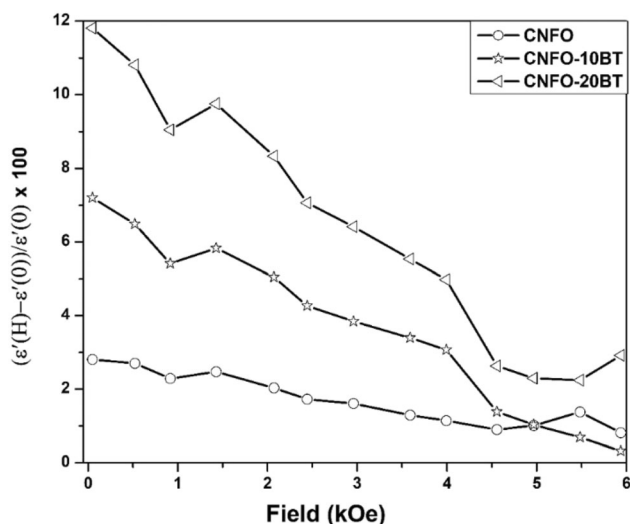


**Fig. 4** Percentage change in dielectric constant for CNFO and CNFO–BT composites as a function of magnetic field at 10 kHz

strain induced in CNFO phase on application of magnetic field creating a mechanical coupling between dielectric and magnetic phases and can be expressed as strain-mediated magnetodielectric response. Additionally, the interfacial polarization effect in CNFO–BT can also induce magnetodielectric behavior based on the impedance of grain or grain boundary with application of magnetic field [41].

Figure 5 shows Nyquist plots of CNFO and CNFO–BT composites. All the composites display single semicircular arc starting from the origin whose radius decreases with temperature suggesting dominance of grains contribution and negative temperature coefficient of resistance [42]. It is noted that the impedance value in the composites increases with BT suggesting highly resistive nature of CNFO–BT composites [43]. CNFO is a weak ferroelectric and poor dielectric material. Thus, the significant contribution in the dielectric and impedance properties is due to the effective content of BTO. Increasing the amount of BTO in CNFO–BT composite therefore increases the net impedance of CNFO–BT composite [43]. The centers of semicircles are observed to be positioned below the  $Z'$ -axis owing from spread relaxation times and indicate the existence of non-Debye relaxations in CNFO–BT composites [44]. The non-Debye relaxations can be understood by representing the Nyquist plots in terms of modified R–C electric circuits. These electric circuits contain arrangement of one or more subarray of resistance ( $R$ ), capacitance ( $C$ ) and constant phase element (CPE) with each subarray denoting the contributions of grains and grain boundary. The non-Debye behavior present in BT–CFO composites is justified from the presence of CPE in the equivalent circuit, which is related to the impedance by the equation  $Z_{\text{CPE}} = 1/(j\omega)^n$  CPE. The corresponding fitted parameters are displayed in Table 1. The impedance spectra of CNFO–BT composites are fitted with one R–CPE parallel combination and are in agreement with each other. The fitting also confirms the dominance of grain resistance in the conduction phenomena.

Figure 6 shows magnetic hysteresis curves for CNFO and CNFO–BT composites. Inset of Fig. 6 shows the enlarged view of M–H curves at low magnetic fields. All composites display systematically strong ferromagnetic behavior. The saturation magnetization for CNFO is comparable to the earlier reported work [25]. However, the saturation

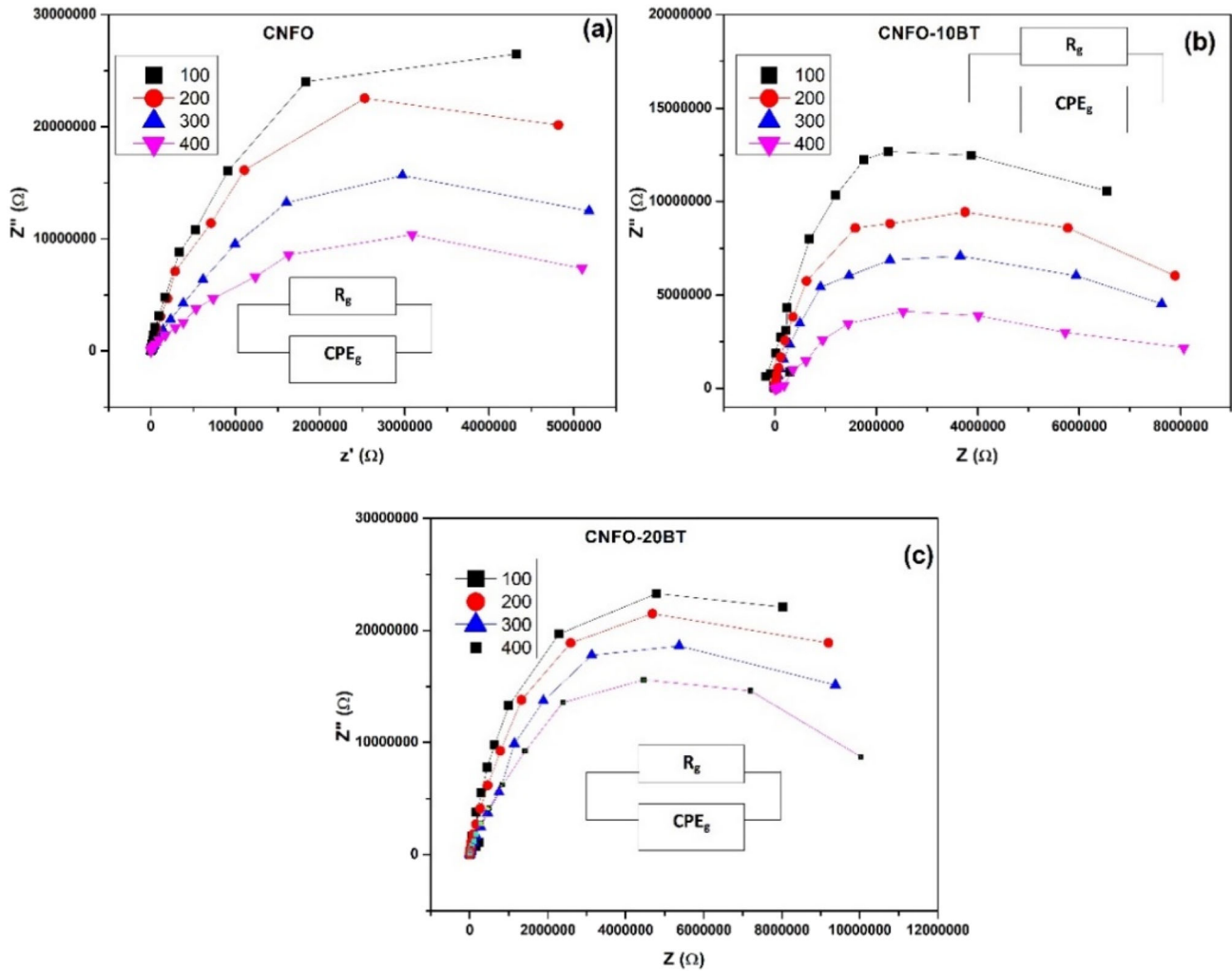


**Fig. 5** Nyquist plot of CNFO–BT composites measured at different temperatures along with their equivalent circuit measured

**Table 1** Fitted parameters for Cole–Cole plots of CNFO–BT composites

Temp (°C)	$R_g$ ( $\Omega$ )	$CPE_g$	$n_g$
<b>CNFO</b>			
200	$6.1 \times 10^6$	$2 \times 10^{-8}$	0.65
300	$4.3 \times 10^6$	$6 \times 10^{-9}$	0.78
400	$1.9 \times 10^6$	$9 \times 10^{-10}$	0.86
<b>CNFO–10BT</b>			
200	$8.2 \times 10^6$	$1.2 \times 10^{-9}$	0.62
300	$5.3 \times 10^6$	$5 \times 10^{-9}$	0.70
400	$3.1 \times 10^6$	$7 \times 10^{-10}$	0.79
<b>CNFO–20BT</b>			
200	$8.9 \times 10^6$	$3 \times 10^{-8}$	0.55
300	$5.4 \times 10^6$	$7 \times 10^{-8}$	0.69
400	$2.9 \times 10^6$	$4 \times 10^{-9}$	0.75

magnetization is smaller than CNFO prepared by different methods [45, 46] which could be due to less duration mixing of primary constituents resulting in incomplete homogeneity of the structure [25]. The magnetic retentivity is found to decrease with increase in content of BT. This re-emphasizes structural distortion induced in CNFO lattice owing to BT substitution. Contrarily, the coercivity is large for CNFO–10BT and least for CNFO–20BT as compared to CNFO. The increased value of coercivity in CNFO–10BT composite is due to enhancement in magneto-electric coupling; however, such coupling is limited by lattice distortion and weakens the ferromagnetic nature in CNFO–BT composite. On further increasing the BT content as in case of CNFO–20BT, enlarged strain-mediated magnetoelectric coupling at the piezoelectric–piezomagnetic interface enhances the ferromagnetic nature.

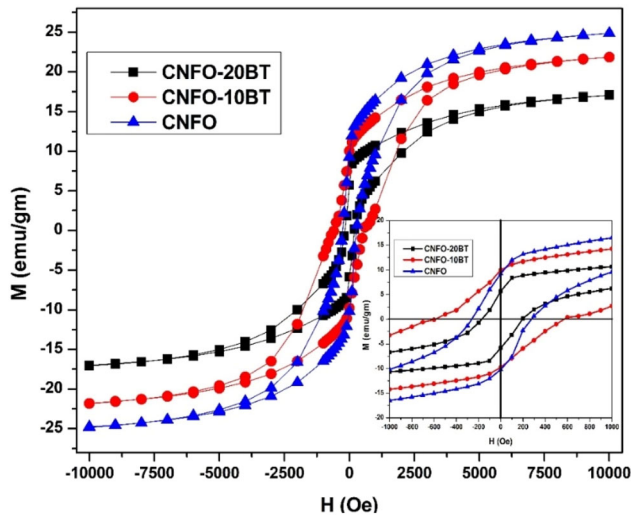


**Fig. 6** Room temperature magnetization curves ( $M$  vs.  $H$ ) for CNFO and CNFO–BT composites. Inset shows the enlarged view of CNFO and CNFO–BT composites

The ferroelectric hysteresis  $P$ – $E$  loops of CNFO–BT composites are plotted in Fig. 7. All the loops show weak  $P$ – $E$  ferroelectric polarization loop because of spatially distributed electric dipoles. The unsaturated lossy  $P$ – $E$  hysteresis loop is originated due to the oxygen vacancies and further to high leakage current in the composites. These oxygen vacancies have been created during synthesis of single oxidized ions of Fe and Ti atoms and are expressed by Kroger–Vink notation

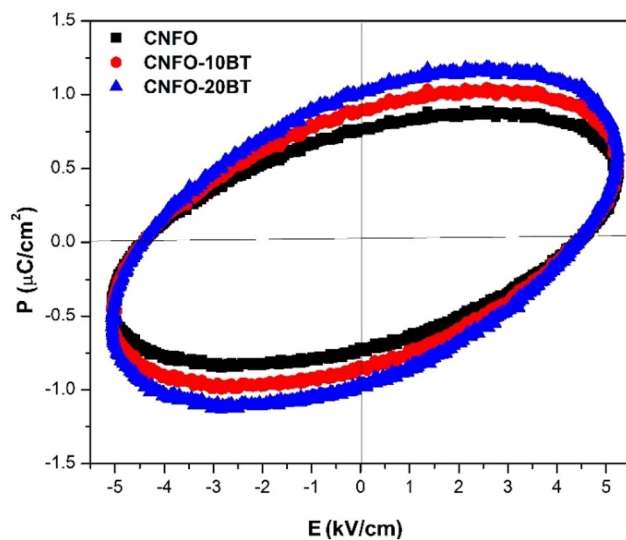


**Fig. 7**  $P$ – $E$  hysteresis loops of CNFO and CNFO–BT composites

where  $V_o^{**}$  is the ionized metal [47]. The magnetic nature of CNFO particles tends to agglomerate and thereby induces weak ferroelectricity [23, 30]. As the content of BT phase is increased in CNFO, the maximum polarization is increased due to increased conductivity. The energy storage and efficiency are estimated from ferroelectric measurements [48]. The unloaded sample of CNFO and CNFO–20BT displayed the energy density of 2.1 and 4.25  $\text{mJ}/\text{cm}^3$ , respectively, with an efficiency of 17 and 31.6%, respectively.

The magnetoelectricity in CNFO–BT composites can be understood well by examining the variation of maximum electric polarization versus applied electric field hysteresis graphs as a function of external magnetic field [49]. Figure 8 shows the variation in maximum polarization measured from  $P$ – $E$  hysteresis loop at different magnetic fields for CNFO and CNFO–BT composites at room temperature with fixed frequency of 50 Hz. The maximum polarization observed decreases with increasing magnetic field suggesting strong magnetoelectric character in CNFO composites. The largest change in maximum polarization of 20% is observed in CNFO–20BT composite, making it most suitable for magnetoelectric devices [50]. This enhanced magnetoelectric effect is correlated with lattice shrinkage on BT substitution resulting in strain-mediated magnetoelectric coupling at the piezoelectric–piezomagnetic interface [26]. In order to obtain the ME coupling coefficient, the variation of  $P_{\text{max}}$  was linearly fitted with magnetic field  $H$ . The error bars obtained from linear fit

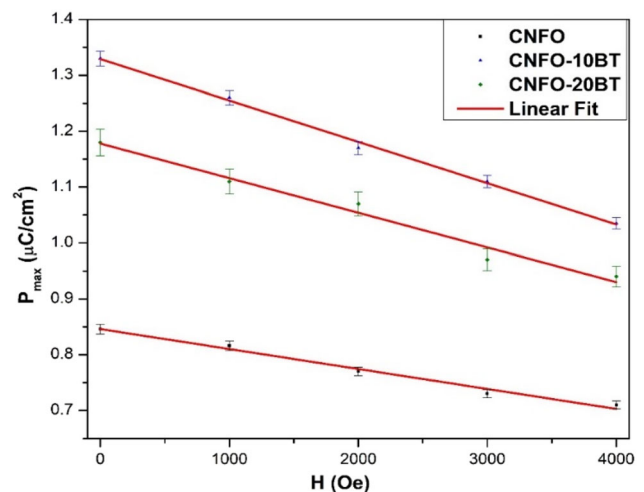


**Fig. 8** Variation of maximum polarization ( $P_{\text{max}}$ ) with magnetic field for CNFO and CNFO–BT composites

are also incorporated in the experimental data plot. The maximum magnetoelectric coupling coefficient ( $\alpha$ ) was achieved for CNFO–20BT composite as 5 mV/cm/Oe. This magnetoelectric response of CNFO–BT composite agrees with some reported results [29, 43].

## 4 Conclusions

$\text{Co}_{0.5}\text{Ni}_{0.5}\text{Fe}_2\text{O}_4$  and  $(1-x)\text{Co}_{0.5}\text{Ni}_{0.5}\text{Fe}_2\text{O}_4-x\text{BaTiO}_3$  (CNFO–BT) magnetoelectric composites were synthesized from solid-state reaction route. The XRD studies reveal lattice distortion and increased strain with BT substitution due to formation of trapping centers in CNFO. The dielectric and impedance measurements reveal presence of interfacial polarization and non-Debye relaxations in CNFO–BT composites. The occurrence of ferroelectric and ferromagnetic hysteresis loops establishes the multiferroic nature in CNFO–BT composite. The evidence of magnetoelectric coupling in CNFO–BT composites is confirmed from magnetodielectric coupling and magnetic-dependent ferroelectric measurements. These results are useful for technological advancements of CNFO–BT composites in magnetoelectric device applications.

## Acknowledgements

This work is funded by Research Scheme no. 03(1427)/18/EMR-II, CSIR, New Delhi, and supported by USIC, University of Delhi, New Delhi, India, for characterization facilities. The authors are also thankful to Netaji Subhas University of Technology (NSUT), New Delhi, India, for  $P$ – $E$  characterization facility and University Science Instrumentation Centre (USIC), University of Delhi, Delhi, India, for XRD and magnetic characterization facility.

## References

1. S. Mohan, P.A. Joy, *Ceram. Int.* **45**, 12307 (2019)
2. M.D. Chermahini, M.M. Shahraki, M. Kazazi, *Mater. Lett.* **233**, 188 (2018)
3. Y. Shu, Q. Ma, Z. Ding, L. Cao, X. Chen, F. Yang, *Phys. Lett. A* **383**, 911 (2019)
4. S. Shankar, M. Kumar, A.K. Ghosh, O.P. Thakur, M. Jayasimhadri, *J. Alloys Compd.* **779**, 918 (2019)
5. S. Liu, S. Yan, H. Luo, S. Huang, C. Liao, L. Deng, *Mater. Lett.* **212**, 139 (2018)
6. S. Lather, A. Gupta, J. Dalal, V. Verma, R. Tripathi, A. Ohlan, *Ceram. Int.* **43**, 3246 (2017)
7. J. Wang, F. Zhao, W. Wu, S. Cao, G. Zhao, *Phys. Lett. A* **376**, 547 (2012)
8. V.K. Chakradhary, A. Ansari, M.J. Akhtar, *J. Magn. Magn. Mater.* **469**, 674 (2019)
9. C. Schmitz-Antoniak, D. Schmitz, P. Borisov, F.M.F. de Groot, S. Stienen, A. Warland, B. Krumme, R. Feyerherm, E. Dudzik, W. Kleemann, H. Wende, *Nat. Commun.* **4**, 2051 (2013)
10. A. Manjeera, M. Vittal, V.R. Reddy, G. Prasad, G.S. Kumar, *Ferroelectrics* **519**, 15 (2017)
11. M.T. Rahman, C.V. Ramana, *J. Appl. Phys.* **116**, 164108 (2014)
12. M. Kumar, S. Shankar, O.P. Thakur, A.K. Ghosh, *Mater. Lett.* **143**, 241 (2015)
13. S. Chandarak, A. Ngamjarurojana, S. Srilomsak, P. Lao-ratanakul, S. Rujirawat, R. Yimnirun, *Ferroelectrics* **410**, 75 (2010)
14. M.U.D. Rather, R. Samad, B. Want, *J. Mater. Sci. Mater. Electron.* **29**, 19164 (2018)
15. N. Ortega, A. Kumar, P. Bhattacharya, S.B. Majumder, R.S. Katiyar, *Phys. Rev. B - Condens. Matter Mater. Phys.* **77**, 1 (2008)
16. R.K. Singh, S. Sanodia, N. Jain, R. Kumar, *AIP Conf. Proc.* **1953**, 1 (2018)
17. S. Shankar, O.P. Thakur, M. Jayasimhadri, *Mater. Chem. Phys.* **234**, 110 (2019)
18. M.P.K. Sahoo, Y. Zhang, J. Wang, *Phys. Lett. A* **380**, 299 (2015)
19. R. Pandey, L.K. Pradhan, S. Kumar, M. Kar, *J. Alloys Compd.* **762**, 668 (2018)
20. P. Liu, Z. Yao, V.M.H. Ng, J. Zhou, L.B. Kong, *Mater. Lett.* **248**, 214 (2019)
21. P. Liu, Z. Yao, J. Zhou, Z. Yang, L.B. Kong, *J. Mater. Chem. C* **4**, 9738 (2016)
22. Manjusha, K.L. Yadav, *J. Mater. Sci. Mater. Electron.* **27**, 6347 (2016)
23. G.D. Dwivedi, K.F. Tseng, C.L. Chan, P. Shahi, J. Lourembam, B. Chatterjee, A.K. Ghosh, H.D. Yang, S. Chatterjee, *Phys. Rev. B - Condens. Matter Mater. Phys.* **82**, 3 (2010)
24. P. Puliová, J. Kováč, A. Voigt, P. Raschman, *J. Magn. Magn. Mater.* **341**, 93 (2013)
25. M.D. Chermahini, H.A. Baghbaderani, M.M. Shahraki, M. Kazazi, *Ceram. Int.* **45**, 5491 (2019)



26. D. Zhang, J. Cheng, J. Chai, J. Deng, R. Ren, Y. Su, H. Wang, C. Ma, C.S. Lee, W. Zhang, G.P. Zheng, M. Cao, *J. Alloys Compd.* **740**, 1067 (2018)
27. N. Pulphol, R. Muanglua, S. Niemcharoen, W. Pecharapa, W.C. Vittayakorn, N. Vittayakorn, *Adv. Mater. Res.* **802**, 22 (2013)
28. N. Pulphol, R. Muanglua, S. Niemcharoen, N. Vittayakorn, W. Vittayakorn, *Ferroelectrics* **488**, 170 (2015)
29. S. Pachari, S.K. Pratihari, B.B. Nayak, *RSC Adv.* **5**, 105609 (2015)
30. R. Gao, Q. Zhang, Z. Xu, Z. Wang, C. Fu, G. Chen, X. Deng, X. Luo, Y. Qiu, W. Cai, *J. Mater. Sci. Mater. Electron.* **30**, 10256 (2019)
31. M. Parshani, M. Nadafan, Z. Dehghani, R. Malekfar, G.H.H. Khorrami, *Results Phys.* **7**, 3619 (2017)
32. B.D. Cullity, *Elements of X-Ray Diffraction*, 2nd edn. (Addison-Wesley Publishing Company Inc, New York, 1978)
33. V. Mote, Y. Purushotham, B. Dole, *J. Theor. Appl. Phys.* **6**, 6 (2012)
34. N. Kasapoglu, B. Birs, *Cent. Eur. J. Chem.* **5**, 570 (2007)
35. A. Kumar, P. Sharma, D. Varshney, *Ceram. Int.* **40**, 12855 (2014)
36. S. Xavier, S. Thankachan, B.P. Jacob, E.M. Mohammed, *IOP Conf. Ser. Mater. Sci. Eng.* **73**, 012093 (2015)
37. S. Thankachan, B.P. Jacob, S. Xavier, E.M. Mohammed, *J. Magn. Magn. Mater.* **348**, 140 (2013)
38. R. Debnath, S.K. Mandal, A. Nath, *Mater. Lett.* **237**, 80 (2019)
39. C.G. Koops, *Phys. Rev.* **83**, 121 (1951)
40. A. Jain, A.K. Panwar, A.K. Jha, *Mater. Res. Bull.* **100**, 367 (2018)
41. G. Catalan, *Appl. Phys. Lett.* **88**, 1 (2006)
42. S. Shankar, M. Kumar, S. Kumar, O.P. Thakur, A.K. Ghosh, *J. Alloys Compd.* **694**, 715 (2017)
43. R. Gao, Q. Zhang, Z. Xu, Z. Wang, G. Chen, X. Deng, C. Fu, W. Cai, *Compos. Part B Eng.* **166**, 204 (2019)
44. M. Kumar, S. Shankar, S. Brijmohan, O.P. Kumar, Thakur, A.K. Ghosh, *Phys. Lett. A* **381**, 379 (2017)
45. Z.H. Low, I. Ismail, M.S.E. Shafie, I.R. Ibrahim, M. Ertuğrul, R.S. Azis, N. Mohd Saiden, I.H. Hasan, F. Mohd, Idris, R. Nazlan, *Results Phys.* **15**, 102683 (2019)
46. G. Muscas, G. Concas, S. Laureti, A.M. Testa, R. Mathieu, J.A. De Toro, C. Cannas, A. Musinu, M.A. Novak, C. Sangregorio, S.S. Lee, D. Peddis, *Phys. Chem. Chem. Phys.* **20**, 28634 (2018)
47. S. Shankar, O.P. Thakur, M. Jayasimhadri, *J. Electron. Mater.* **49**, 472 (2020)
48. S. Shankar, M. Kumar, V. Tuli, O.P. Thakur, M. Jayasimhadri, *J. Mater. Sci. Mater. Electron.* **29**, 18352 (2018)
49. M. Kumar, S. Shankar, R.K. Kotnala, O. Parkash, *J. Alloys Compd.* **577**, 222 (2013)
50. M. Sufyan, S. Atiq, S.K. Abbas, M. Younis, *Mater. Lett.* **238**, 10 (2018)

**Publisher's Note** Springer Nature remains neutral with regard to jurisdictional claims in published maps and institutional affiliations.